

THE REACTION OF Fe AND Ni AT INTERMEDIATE ENERGIES

A Senior Honor Thesis

By

SEAN NICHOLAS LIDDICK

Submitted to the Office of Honors Program
& Academic Scholarships
Texas A&M University
In partial fulfillment of the requirements of the

UNIVERSITY UNDERGRADUATE
RESEARCH FELLOWS

April 2001

Group:
Physical Sciences

THE REACTION OF Fe AND Ni AT INTERMEDIATE ENERGIES

A Senior Honors Thesis

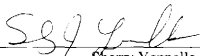
By

SEAN NICHOLAS LIDDICK

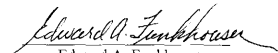
Submitted to the Office of Honors Program
& Academic Scholarships
Texas A&M University
In partial fulfillment of the requirements of the

UNIVERSITY UNDERGRADUATE
RESEARCH FELLOWS

Approved as to style and content by:



Sherry Yennello
(Fellows Advisor)



Edward A. Funkhouser
(Executive Director)

April 2001

Group: Physical Sciences

ABSTRACT**The Reaction of Fe and Ni at Intermediate Energies (April 2001)**

Experimentally and theoretically, the affect of isospin on nuclear reactions has been studied intensively. Among the affects that have been observed to affect reactions are neutron number and size of the reaction system. In this thesis work the focus was on systems of constant mass but varying neutron to proton ratio. The three main reaction systems that were studied were the following: $^{58}\text{Fe} + ^{58}\text{Fe}$, $^{58}\text{Fe} + ^{58}\text{Ni}$, $^{58}\text{Ni} + ^{58}\text{Ni}$, at energies of 35 and 45 MeV. The reaction was carried out at the Texas A&M University Cyclotron Institute. Differing beams of the above materials were created and impinged on the different targets. The resulting fragments were detected in combinations of cesium iodide detectors, silicon detectors and the neutron ball. Some of the observables that were studied from these different reactions were neutron and charged particle multiplicities and information on the isotopic composition of the fragments. The data show that the neutron multiplicity increases with increasing neutron to proton ratios. The isotopic distribution was also shown to depend on the neutron multiplicity of the reaction, the angle of detection, and the energy of the incident beam.

Sean Nicholas Liddick
Department of Chemistry
Texas A&M University

Fellows Advisor: Dr. Sherry Yennello
Department of Chemistry

TABLE OF CONTENTS

	Page
ABSTRACT.....	iii
TABLE OF CONTENTS.....	iv
LIST OF FIGURES.....	v
INTRODUCTION.....	1
EXPERIMENT.....	3
Detectors.....	4
Cesium Iodide.....	4
Silicon Detector.....	8
Neutron Ball.....	9
ANALYSIS.....	10
Multiplicities of Neutrons, Light Fragments, and IMF's.....	10
Isotopic Ratios.....	14
SUMMARY AND CONCLUSIONS.....	23
REFERENCES.....	25
VITA.....	26

LIST OF FIGURES

FIGURE	Page
1. Schematic of NIMROD.....	4
2. Diagram of a Cesium Iodide Band Gap.....	5
3. Pulse Shape Discrimination.....	6
4. Photomultiplier Tubes.....	7
5. Silicon Detector under Reverse Bias.....	8
6. Slow-Fast Plot of the Cesium Iodide detector.....	11
7. Neutron versus Charged Particle Multiplicity.....	12
8. Intermediate Mass Fragments as a Function of Charged Particle Multiplicity.....	13
9. Silicon Silicon Plots.....	15
10. Fit of Energy Loss Calculations in Silicon Detectors.....	16
11. Isotope Ratios as a Function of Multiplicity.....	20
12. Isotope Ratio as a Function of Detection Angle.....	21
13. Isotope Ratio as a Function of Beam Energy.....	22

INTRODUCTION

Nuclear reactions during the lives and deaths of stars have produced all of the naturally occurring elements. The relative abundances of the different elements are determined by the reaction mechanism governing these different processes. In order to understand processes such as supernovae, and the elemental abundances that come out of such processes, it is important to determine the characteristics of the many different nuclear reactions. To do this, laboratory reactions can be used to gain additional information, such as the dependence of the isotopic distribution of the fragments on the initial nuclei and their energy. This will aid in the many theoretical calculations needed to model astrophysical processes. The Texas A&M University Cyclotron was employed for this purpose to study different reactions of Ni and Fe.

In recent years much attention has been paid, both experimentally and theoretically, to the isospin of a reacting system and its effect on the reaction mechanism [1-4]. The isospin is a quantum mechanical property of a type of particle called a nucleon. Protons and neutrons are the two types of nucleons that can only be differentiated from each other by their isospins. For a neutron the isospin is defined to be $+1/2$ and for a proton it is defined as $-1/2$, [much the same way as the electron spin is defined to be $\pm 1/2$]. The related variable that was experimentally altered in this thesis work was the neutron to proton ratio of the reaction system. It has been previously shown that the size and the neutron to proton ratio of the reacting system are important [1,5-6] to the multiplicity of emitted fragments.

This thesis follows the style and format of Physics Review C.

In the previous studies the neutron number of the system was varied which in turn altered the size of the reacting system. These two effects, the size and the neutron number, were linked together and could not be decomposed into two different factors. In this thesis work the effect of the isospin was studied across a variety of systems that kept the total size of the system constant in an effort to minimize the uncertainties found in Kunde's research. The current study focused on systems of constant mass but varying neutron to proton ratio. The three main reaction systems that were studied were the following: $^{58}\text{Fe} + ^{58}\text{Fe}$, $^{58}\text{Fe} + ^{58}\text{Ni}$, $^{58}\text{Ni} + ^{58}\text{Ni}$. By using mass 58 for these two elements the total size of the system was removed as a variable in the reaction. The neutron to proton ratio of the systems ranges from values of 1.3 to 1.07 respectively. The data that was studied from these different reactions was neutron and charged particle multiplicity, where multiplicity is the total number, of the particle in question, given off by the reaction, and information on the isotopic composition of the fragments. The multiplicities were obtained from the cesium iodide detectors (CsI) and the neutron ball, the operation of which will be described in the Experimental section. Isotopic information from the silicon detectors, also to be discussed in the Experimental section, was used to analyze the isotopic ratios of the different isotopes of boron, carbon, and nitrogen.

EXPERIMENTAL

The data were taken at the Texas A&M University Cyclotron. Two different beams of ^{58}Fe and ^{58}Ni were accelerated to two different energies of 35 and 45 MeV, millionelectron volt, inside the K500 Superconducting cyclotron. These beams were then guided from the cyclotron to the NIMROD, Neutron Ion Multidetector for Reaction Oriented Dynamics, setup to impinge on self supporting foils of thickness 1.0 and 1.7 mg/cm^2 for ^{58}Fe and ^{58}Ni , respectively. NIMROD consists of ion chambers, silicon, and cesium iodide detectors arranged into 4 different circular rings. These different rings were stacked together to form a cylinder. The entire cylinder, marked as rings 2 through 9 in figure 1, was placed inside the neutron ball. To augment this the CsI Ball will be used for the backward angles, rings 10 through 13 in the figure. In this manner, angular coverage from 3.6 to 170 degrees was achieved. In the following sections the basic characteristics of each type of detector will be discussed.

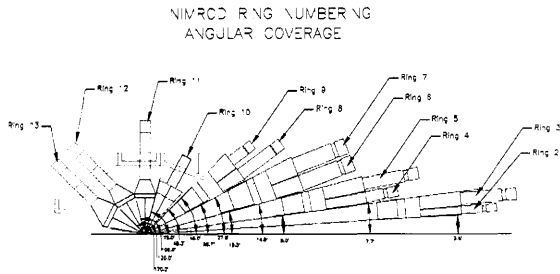


Figure 1: A schematic along the long axis of the cylinder of the NIMROD. The neutron ball is omitted for clarity. The two angles of detectors that were used for the isotopic analysis are the labeled rings 23 and 67 and have angles of $3.4 - 7.7$ and $15.3 - 27.8$ degrees respectively.

Cesium Iodide

A cesium iodide detector is a crystalline solid, which can be created in a variety of shapes. The cesium iodide (CsI) was doped with a small amount of thallium: its purpose is to introduce different activator levels into the CsI band gap structure. When radiation enters the detector the first process that occurs is the promotion of an electron from the valence band to the conductance band of the material. This promoted electron then decays back down to one of the activator levels provided by the thallium. After this initial

deexcitation, the electron then decays all the way back down to the ground state and emits a photon of light.

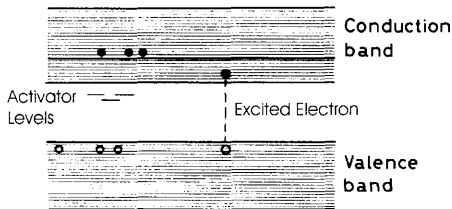


Figure 2: Adapted from Leo [7]. A characteristic band gap diagram for a CsI detector doped with a small amount of thallium to impart different activator levels to the detector.

To be useful there must be a way to tell different particles apart based on their light output. To differentiate between different particles emitted in the reaction a technique called pulse shape discrimination is used. The light that is emitted from an emitted particle in the CsI detector first rises very quickly and then slowly decays away. The total signal as well as its decomposition into the slow and fast contributions is shown in figure 3.

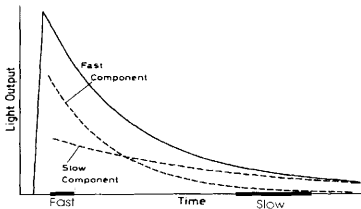


Figure 3: From Leo [7]. The decomposition of the total signal into its slow and fast components.

Gates are placed on the fast and slow portion of the light curve, marked as slow and fast in the figure, and the respective signal is integrated between the limits. Different particles have different light curves and by plotting the relative amounts of the slow and the fast signal of the CsI it becomes possible to differentiate between different particle types.

To turn the light into a usable electric signal a photomultiplier tube (PMT) is used. In this tube, a photon first hits a photoelectrode that will emit an electron. This electron is then accelerated to the dynodes where it is multiplied and sent toward the next dynode where the process repeats. This continues until the electrons hit a collector at the end of the PMT and the electrical signal is produced.

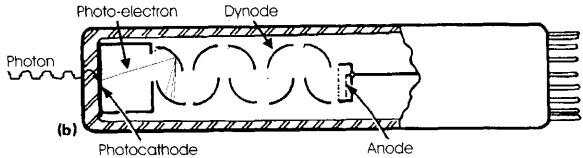


Figure 4: Adapted from Leo [7]. A photomultiplier tube with the path of a photon and photoelectron shown.

The CsI detectors that comprise NIMROD have the following characteristics:

1. The detectors for rings 2-5 (review figure 1), 6 and 7, and 8 and 9 are 100, 65, and 60 mm thick respectively. The detectors for rings 10-13 range between 10 and 30 mm thick.
2. The CsI crystals are tightly wrapped in Teflon tape. This prevents the loss of light by providing more internal reflection. The Teflon also protects the crystals from atmospheric water, as they are hygroscopic.
3. The front surface of the crystal is covered with a thin sheet of mylar for two reasons. The first is to keep light that is inside the detector from escaping and the second is to prevent light outside the detector from interfering with the measurement.
4. The PMT is glued to the end of the CsI by special optical glue. Care was taken to ensure that no air remained trapped between the PMT and the CsI because this reduces the efficiency of the detector.

Silicon Detectors

A silicon detector is just a semiconductor pn junction. This junction is placed under a reverse bias (see fig 6) to create a depleted region, a region of few charge carriers, in the detector that is the sensitive volume of the detector.

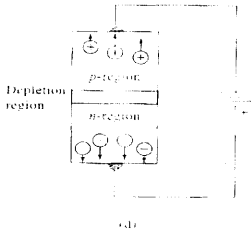


Figure 5: adapted from Skoog [9]. A schematic showing the p and n region of a silicon detector under a reverse bias to create a depleted region in the detector.

When radiation enters this sensitive volume, positive and negative charges were developed and migrated to their respective electrodes and caused a small change in the electric signal. NIMROD has two types of silicon telescopes. The first contain only a single silicon detector and is either 150 or 300 μm thick. The other telescope, the supertelescope, has two silicon detectors of thickness 150 and 500 μm stacked back to back.

It is the supertelescopes that were used for the isotopic identification of the fragments emitted in the reaction. The radiation coming into the first silicon detector deposits a small amount of energy (ΔE). The particle then enters the second detector and can either deposit the remainder of its energy and stop in the second silicon (E) or deposit another portion of its energy and then punch through to the CsI detectors. When the quantity of E was plotted against ΔE it became possible to differentiate not only different elements but also their respective isotopes.

Neutron Ball

The neutron ball is a large segmented tank filled with an organic compound. The organic compound used in this experiment is pseudocumene doped with a small amount of gadolinium. When a neutron enters the tank it excites a gadolinium molecule into an excited state that then decays back down to the ground state with the emission of a gamma ray. This gamma ray then excites the pseudocumene, which then releases a photon when it decays back down to the ground state. The light is collected by PMTs as in the CsI detectors where it is turned into a usable signal.

Analysis

The reaction particles were detected in different combinations of detectors and complimentary information was obtained from each of these detectors. For the present analysis the CsI and silicon supertelescopes will be used. For the CsI analysis all of the CsI detectors contained inside NIMROD will be used, which provided information concerning the light charged particles. The silicon supertelescopes produced the isotopic information and were studied at two different experimental angles of $3.4 - 7.7$ and $15.3 - 27.8$ degrees.

Multiplicities of Neutrons, Light Fragments, and IMFs

By using the technique of pulse shape discrimination as previously described and plotting the slow signal versus the fast signal of the detector a graph was obtained that allows for the easy identification of the isotopes of hydrogen and helium as shown in the following graph:

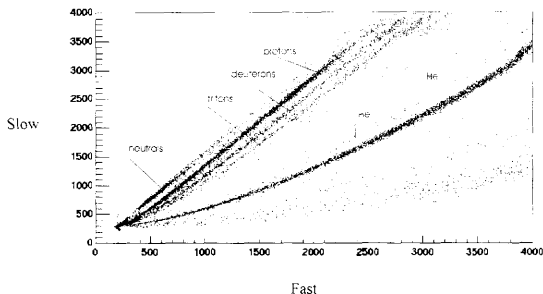


Figure 6 A typical Slow/Fast plot from a CsI detector. The light particles were resolved in this type of detector and the neutrals as well as the isotopes of hydrogen and helium can be seen clearly.

In order to obtain a graph of the neutron multiplicity, the number of emitted neutrons N_n , was plotted against the charged particle multiplicity, N_c . For subsequent analysis the charged particles in the graph above must be identified and counted. This was accomplished by drawing a box around the neutrons and gamma rays and subtracting them from the total number of particles detected inside NIMROD for each reaction. The neutron multiplicity was obtained from the neutron ball and plotted against the value of N_c . This information is plotted in figure 8 for the $^{58}\text{Fe} + ^{58}\text{Fe}$ systems.

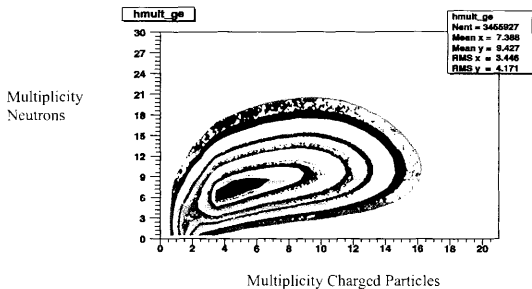


Figure 7 The N_n plotted as a function of N_c for the $^{58}\text{Fe} + ^{58}\text{Fe}$ reaction system.

From the contour plots above the average number of neutrons for each given charged particle number can be determined. This relationship is shown for all reactions systems in the following figure.

Multiplicity Neutrons vs Charged Particles

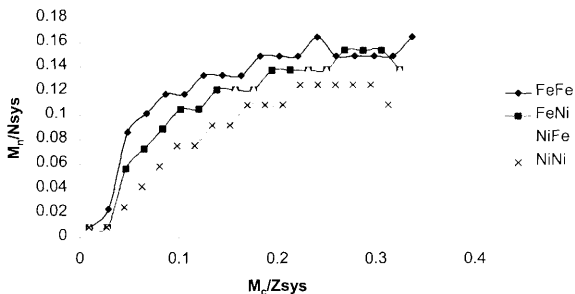


Figure 8: N_n plotted as a function of charged particles for the four different reaction systems. The errors in M_n/N_{sys} are estimated to be no greater than 0.008 units.

The $^{58}\text{Ni} + ^{58}\text{Ni}$ system had about 8% more charge available for the production of charged particles as compared to the $^{58}\text{Fe} + ^{58}\text{Fe}$ system. This could bias the nickel system toward larger values of N_c . To compensate for this, the x-axis was normalized by dividing the values on the x by the total charge of the system. Similarly the values on the y-axis were normalized by dividing by the total neutron number of the system. From the graph it can be seen that the more neutron rich systems preferentially give off more neutrons, in concordance with the results of Dempsey and Kunde[10,5]. What is interesting about the current work was that it included the two different cross systems of $^{58}\text{Fe} + ^{58}\text{Ni}$ and $^{58}\text{Ni} +$

^{58}Fe . These two systems should give the same composite nucleus if everything came to equilibration before particle emission. This would mean that if this is the correct picture then the two lines should lie on top of each other, which they do not. One explanation for the shift in the two curves, even though they have the same isospin, is that the detector acceptance could vary inside NIMROD between the forward and backward angles. The detectors might be able to accept the same amount of energy in the lab but when this energy is converted into the center of mass energies, the backwards angles might have a much higher energy threshold. A second effect, which could be driving the difference between the two identical isospin systems, is the degree of equilibration in the formation of the composite nucleus. Previous studies [11-12] have already determined that the energy range of this experiment is one in which a complete equilibration of the interacting nuclei should not be expected. Any differential shift in the acceptance coupled with some amount of nonequilibration would result in the shift of the two curves.

Additionally, the plots of the multiplicity of neutrons versus charged particles, are extremely important in event selection where events were characterized by their respective impact parameters. The impact parameter is the distance between the centers of the two nuclei at the point of closest approach. The events that are located on the upper right hand side of the plot are the ones that have the lowest impact parameter, a head on collision, and are therefore more violent releasing more charged particles and neutrons. The ones on the lower left of the reaction are the peripheral events, high impact parameter, that release less neutrons and charged particles.

Isotopic Ratios

To try and determine the effect of the isospin on the reacting system, attention was turned to isotope yields for the different reactions. For the following analysis the E-E plots derived from silicon detectors were used. From these plots the isotopes of boron, carbon and nitrogen were well resolved and relatively free from noise.

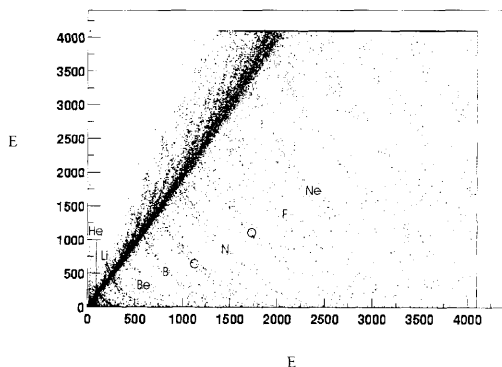


Figure 9: A E-E plot derived from the silicon silicon detectors showing isotopic resolution.

For each reaction system these fragments were isotopically identified. For this a method was developed for particle identification. The starting point of this identification

was the theoretical description the energy loss of different particles inside all of the major elements inside NIMROD. This included energy loss calculations inside the gas ionization chamber as well as the energy loss in both silicon detectors and the CsI detectors. The calculated energy loss through the two silicon detectors was plotted and these theoretical lines were then fitted with a sixth power polynomial, see figure 10 using ^{12}C as an example, of the form: $E = a\Delta E^6 + b\Delta E^5 + c\Delta E^4 + d\Delta E^3 + e\Delta E^2 + f\Delta E + g$.

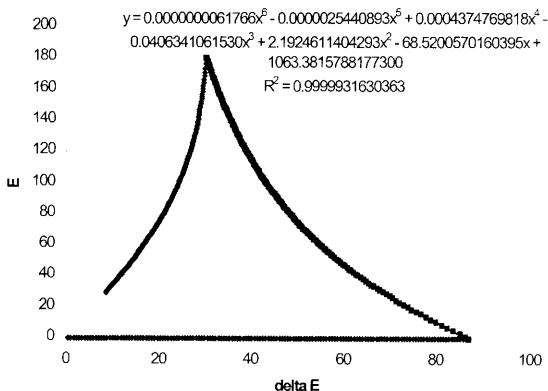


Figure 10: Plotting the energy loss of a ^{12}C particle inside the two silicon detectors and the polynomial fit to the region to above the first punch through.

Only the region between the two punch-throughs, in the case of ^{12}C above from approximately 25 to 88 MeV, was used. Higher energy particles that punched through the silicon detectors can be identified inside the CsI detectors. Over the range of interest, the sixth order polynomial is a strictly monotonic function. The distance between any point, (x_1, y_1) , and an arbitrary location on the line can be defined as

$$\text{distance} = \sqrt{(x_1 - \Delta E)^2 + (y_1 - (a\Delta E^6 + b\Delta E^5 + c\Delta E^4 + d\Delta E^3 + e\Delta E^2 + f\Delta E + g))^2} \quad (1)$$

By defining some functions the above equation can be simplified into

$$\begin{aligned} f(\Delta E) &= a\Delta E^6 + b\Delta E^5 + c\Delta E^4 + d\Delta E^3 + e\Delta E^2 + f\Delta E + g \\ h(\Delta E) &= x_1 - \Delta E \end{aligned} \quad (2)$$

$$\text{dis tan ce} = [h(\Delta E)^2 + f(\Delta E)^2]^{1/2} \quad (3)$$

The equation for the distance has only one minimum inside the range of interest. To find the minimum of this equation, its derivative was taken while holding the points x_1 and y_1 constant resulting in

$$\text{distance}' = \frac{h(\Delta E) * h'(\Delta E) + f(\Delta E) * f'(\Delta E)}{[h(\Delta E)^2 + f(\Delta E)^2]^{3/2}} \quad (4)$$

When this derivative was equal to zero the shortest distance between the point and the line was obtained. To find the zero of this particular function the denominator can be ignored so we are looking for the zero of the following function.

$$h(\Delta E)h'(\Delta E) + f(\Delta E)f'(\Delta E) \quad (5)$$

In order to find the zero of this function Newton's Method [13] was used. Newton's Method for calculating a zero of a function proceeds as follows. The first requirement of Newton's method is that the function and its derivative be defined and continuous over the entire range of computation. Since our function is a simple polynomial function it satisfies

this criteria. Since the function is also monotonic, there is no need to worry about this method calculating different solutions for different starting points. Beginning with (5) the derivative is computed to be

$$h'(\Delta E) + f(\Delta E)f''(\Delta E) + [f'(\Delta E)]^2 \quad (6)$$

An arbitrary starting point on eq 5 is chosen to begin searching for a zero. The tangent line is computed from the starting point and eq 6. The value where this tangent line is equal to 0 is identified. This point serves as the next starting point for the tangent line calculation and the process is repeated until the numbers before and after the tangent line calculation are within some preset tolerance, defined as 0.000005 for present purposes. It was found that this value led to the least amount of computing time while still ensuring the correct results. Once the zero has been found it is put back into eq 1 to obtain the minimum distance between the point (x_1, y_1) and the line of interest. This procedure is then repeated for the same point over all of the theoretical lines representing the energy loss in the silicon detectors for each isotope. The isotopic line for which the computed distance is the least is taken to be the identification of the particle. In this manner all of the particle above the noise threshold and in the correct region of the graph could be identified and counted. An additional constraint was set on the most neutron rich and the most neutron poor isotope of each element. For these isotopes the maximum distance that an arbitrary point could be from the line and still be identified with that isotope was limited to make sure that each isotope had the same energy width around its isotopic line. This meant that to be identified with any particular isotope a point would have to fall within about 1.3 MeV of a particular isotopic line. This value remained fairly constant for the isotopes that were studied.

The yield of the different isotopes were calculated according to the following formula:

$$\%yield = \frac{\#isotope_particle}{\#element_particle} \quad (7)$$

In this formula the numerator is the total number of particles a given isotope, for example ^{14}C . The denominator is the total number of particles for all the isotopes of the current element; following from the example above this would be all the particles of all C isotopes. Unless otherwise specified all isotope ratios are calculate from the ring 67 data, lab angles between 15.3 and 27.8 degrees.

For the following analysis, different cuts on the neutron multiplicity are made. While a stricter determination of the centrality of the collision could be achieved through the use of cuts on both neutron and charged particle multiplicity for the present purposes the neutron cut was sufficient. The three different cuts were for neutron multiplicities above 10, all multiplicities, and multiplicities below 6. These cuts allowed for the most violent collisions, all collisions, and the most peripheral collisions to be selected respectively (fig 12). The most obvious trend observable was that the more neutron rich the system was, the more that system forms the neutron rich isotopes. The second interesting feature was that for each different element, if the results for the different cuts were plotted for each reaction system it can be seen that the lower the multiplicity, the higher the production of the more neutron rich isotope. This effect can be seen the clearest for the carbon isotopes. This can be understood in the following manner. The lower the multiplicity of the reaction the more peripheral it is. Particles that are emitted from these reactions could be coming from a neck like region, which is predicted to be more neutron rich than the surrounding nuclear material [10].

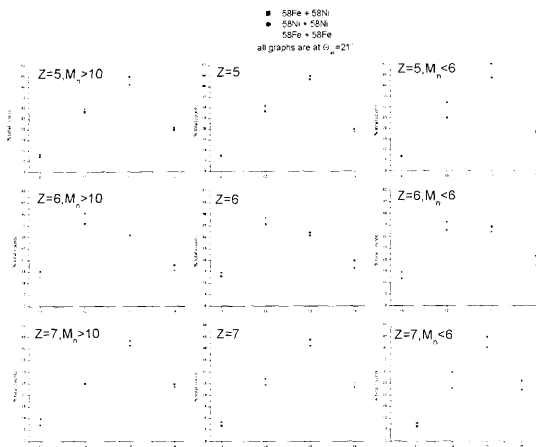


Figure 11: Isotopic distribution of boron (top), carbon (middle), nitrogen (bottom) fragments from the three different reactions at energies 45 MeV for central (left), inclusive (middle), and peripheral (right) collisions.

Another interesting point was that the isotopic distribution also changes as a function of the angle at which the particles are detected. When the reactions are plotted for the two different lab angles of 3.4 – 7.7 and 15.3 – 27.8 degrees it was seen that in the more forward detectors the lighter isotopes were emphasized. This could be due to the fact that the different detectors will sample different portions of the particles energy spectrum and

thus give different results [14], as well as the fact that different reaction mechanisms preferentially populate different angles.

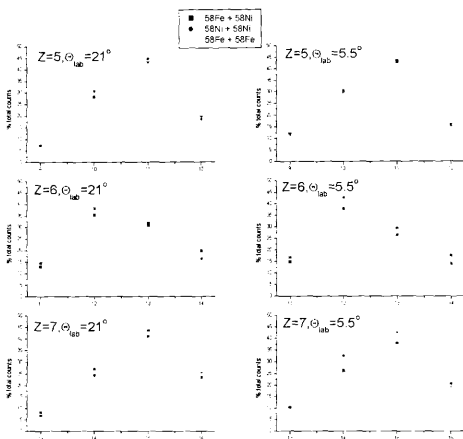


Figure 12: Isotopic distribution of boron (top), carbon (middle), and nitrogen (bottom) fragments for all three reactions at 45 MeV (squares) for ring 23 (left), and ring 67 (right).

The last variable that was analyzed was the energy of the reaction system. For this the reaction $^{58}\text{Fe} + ^{58}\text{Fe}$ was analyzed at energies of 45 and 35 MeV. The isotope ratios for carbon are plotted in figure 13 with the same three multiplicity cuts as in figure 11. From the graph it can be seen that heavier isotopes are enhanced at multiplicities less than 6 and

that this enhancement increases with increasing beam energy. The neutron enhancement of the system can be explained by the fragments coming from a neutron rich material such as a neck source [10]. The neutron enhancement at low multiplicities and at 45 MeV could have to do with a possible coexistence region in which the reaction that might not be present in the 35 MeV data [3].

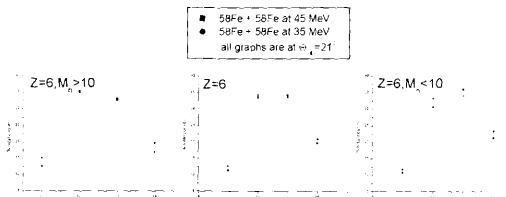


Figure 13: Isotopic distribution of carbon fragments from the reactions of $58\text{Fe} + 58\text{Fe}$ at energies of 35 MeV (circles) and 45 MeV (squares) for central (left), inclusive (middle), and peripheral (right) collisions.

SUMMARY AND CONCLUSION

The reaction of different systems of ^{58}Fe and ^{58}Ni were studied at 35 and 45 MeV to try and gain insight into the effect of isospin on the reaction. Multiplicities of neutrons and charged particles were the first observables that were studied. It was concluded that the more neutron rich the system is the more neutrons are given off during the reaction even after correcting for the number of neutrons available. However, even though two systems might have the same isospin it does not mean that they will have the same profile for the emission of neutrons with respect to charged particles. This can be rationalized when it is taken into consideration that the detector acceptance might not be uniform throughout NIMROD and that the system is most probably not at equilibrium. Due to the peripheral events, which do not collide to create an equilibrated composite nucleus, when the reaction is observed at all multiplicities it is highly probable that the reaction is not at equilibrium. A further factor that could be affecting the difference in the systems is the trigger that were used in the acquisition stage. If a reaction system is triggered on a multiplicity of one and then it is changed to four it can be seen that the higher trigger serves to select more central collisions making the analysis much more complicated. To make further use of the neutron multiplicities, event selection was accomplished on the basis of the number of neutrons emitted and related to the impact parameter of an event. This characterization was useful in the analysis of the variation of the isotope ratios derived from the silicon detectors in going from a central to a peripheral collision. Through theoretical energy loss calculations and the use of Newton's Method all particles detected during the experiment were isotopically identified. The isotopes of boron, carbon, and nitrogen isotopes were chosen for extensive analysis. From this it was seen that there were numerous variables that affect the

distribution of the isotopes for a given element. The first variable studied was the neutron multiplicity of the reaction. As this multiplicity decreased, meaning more peripheral collisions, the heavier isotopes, were preferentially formed which can be explained by the emission of these heavier particles from a neutron rich source, such as a neck like source, inside the interacting system. The isotope ratios favor the neutron poor isotopes at forward angles in the lab frame, possibly due to the sampling of different portions of the particle's energy spectrum in the different detectors and other issues of detector acceptance. A second possible explanation has to do with the manner in which the reaction proceeds. If the projectile is collided with the target at a peripheral impact parameter then this could neck between the two nuclei through which nucleons can be exchanged. If this neck is neutron rich as theory says then these neutrons would have to be stripped from the projectile. The resulting projectile like fragment is neutron poor and has a substantial energy in the forward direction which leads to the favoring of the neutron poorer isotope in the forward angles. The energy of the reaction was also shown to have an effect in the isotope ratios and this is most probably due to the fact that at 35 MeV the system is fairly equilibrated while at 45 MeV it is not.

REFERENCES:

1. M.L. Miller *et al.*, Phys. Rev. Lett. **82**, 1399 (1999)
2. Bao-An Li, C.M. Ko and W. Bauer, Int. Jou. Of Mod. Phys. **E7**, 147 (1998)
3. Ph. Chomaz, F. Gulminelli., Phys. Lett. B. **447**, 221 (1999)
4. M. Veselsky *et al.*, Phys. Rev. C. **62**,
5. G.J. Kunde *et al.*, Phys. Rev. Lett. **77**, 2897 (1996)
6. K. Kwiatkowski *et al.*, Phys. Rev. Lett. **74**, 3756 (1995)
7. Leo, W.R., Techniques for Nuclear and Particle Physics Experiments. Springer-Verlag, New York. 1994
8. Knoll, Glenn F., Radiation Detection and Measurement. John Wiley & Sons, New York. 1989.
9. Skoog, Douglas A., Principles of Instrumental Analysis. Saunders College Publishing, Ft Worth, Tx. 1998.
10. J.F. Dempsey *et al.*, Phys. Rev. C. **54**, 1710 (1996)
11. H. Johnston *et al.*, Phys. Lett. B. **371**, 186 (1996)
12. Bao-An Li, Yennello, Sherry, Phys. Rev. C. **52**, 1746 (1995)
13. Press, William H., Numerical Recipes in FORTRAN. Cambridge University Press, New York, NY. 1992
14. E. Renshaw *et al.*, Phys. Rev. C. **44**, 2618 (1991)

VITA

Sean Nicholas Liddick

4803 Legend Well Dr.

San Antonio, Tx 78247

EDUCATION

B.S. Texas A&M University, Chemistry, May 2001

EXPERIENCE

Undergraduate research at the Texas A&M University from 1998 – May 2001

AWARDS

Outstanding Freshman Undergraduate Chemistry Major

Outstanding Sophomore Undergraduate Chemistry Major

Outstanding Junior Undergraduate Chemistry Major

1st place Baylor ACS Undergraduate Research Competition

PRESENTATIONS

Baylor ACS Undergraduate Research Competition

Presentations for Honors Thesis Group, Physical Sciences

Texas A&M University Student Research Week

Poster Presentation at 2001 Spring ACS National Meeting